Optical and energy-loss spectra of the antiferromagnetic transition metal oxides MnO, FeO, CoO, and NiO including quasiparticle and excitonic effects

Claudia Rödl and Friedhelm Bechstedt

Institut für Festkörpertheorie und -optik, Friedrich-Schiller-Universität and European Theoretical Spectroscopy Facility (ETSF), Max-Wien-Platz 1, 07743 Jena, Germany

(Received 12 October 2012; published 17 December 2012)

We calculate the frequency-dependent dielectric function for the series of antiferromagnetic transition metal oxides (TMOs) from MnO to NiO using many-body perturbation theory. Quasiparticle, excitonic, and local-field effects are taken into account by solving the Bethe-Salpeter equation in the framework of collinear spin polarization. The optical spectra are based on electronic structures which have been obtained using density-functional theory with a hybrid functional containing screened exchange (HSE03) and a subsequent quasiparticle calculation in the GW approximation to describe exchange and correlation effects adequately. These sophisticated quasiparticle band structures are mapped to electronic structures resulting from the computationally less expensive GGA$+U+\Delta$ scheme that includes an on-site interaction U and a scissors shift Δ and allows us to calculate the large number of electronic states that is necessary to construct the Bethe-Salpeter Hamiltonian. For an accurate description of the optical spectra, an appropriate treatment of the strong electron-hole attraction is mandatory to obtain agreement with the experimentally observed absorption-peak positions. The itinerant s and p states as well as the localized transition metal $3d$ states have to be considered on an equal footing. We find that a purely atomic picture is not suitable to understand the optical absorption spectra of the TMOs. Reflectivity spectra, absorption coefficients, and loss functions at vanishing momentum transfer are computed in a wide spectral range and discussed in light of the available experimental data.

DOI: 10.1103/PhysRevB.86.235122 PACS number(s): 71.35.Cc, 71.45.Gm, 78.20.Bh, 75.50.Pp

I. INTRODUCTION

The series of transition metal (TM) oxides (TMOs) from MnO to NiO possesses a unique variety of physical properties.[1] The partially filled $3d$ shells which energetically overlap with the oxygen $2p$ and TM $4s$ states evoke an intricate interplay between lattice, orbital, and spin degrees of freedom. All four materials crystallize in rock-salt structure in their paramagnetic phase. However, below their respective Néel temperatures, they become antiferromagnetic. The magnetic phase transition is accompanied by structural distortions that are not yet fully understood from a theoretical point of view.[2–4]

Despite their only partially filled $3d$ shells, the TMOs are insulating above as well as below the Néel temperature. This surprising behavior has puzzled theoretical physicists since the early days of solid-state physics.[5,6] To describe the peculiar electronic structures of the TMOs, theoretical approaches that treat *both* the itinerant s and p and the strongly localized d states with the same accuracy are indispensable. Historically, two lines of research emerged. One approach started from the atomic states of the TM ions and incorporated the effects of the crystalline environment in a perturbational way, first in cluster approximations,[7] and later by means of a bath in dynamical mean-field theory.[8,9] The second line of research has its origins in semiconductor physics. Band-structure calculations in density-functional theory[10,11] (DFT) using (semi-)local exchange-correlation functionals were carried out for the TMOs.[12] It turned out that a more advanced treatment of exchange and correlation is necessary to obtain band gaps and densities of states in agreement with spectroscopic data, e.g., from photoemission. Nowadays, various approaches that differ in accuracy and computational workload are available: an on-site interaction term U is added to the exchange-correlation functional,[13,14] generalized Kohn-Sham equations with hybrid functionals are solved,[15,16] or many-body perturbation theory in Hedin's GW approximation[17] is applied either in a self-consistent scheme[18] or perturbationally on top of an advanced starting electronic structure.[19–21] The two lines of research basically meet again and describe the electronic structures of the TMOs with comparable precision. However, the TMOs are still considered a stringent test bed for new methods in electronic-structure theory.

Considering the strong research activity to understand the one-particle excitation properties of the TMOs, in particular the band gaps and photoemission spectra, it is rather surprising how little attention has been paid to the calculation of their optical properties. The absorption spectra of these materials have been measured decades ago,[22–24] but have not yet been explained satisfactorily by means of state-of-the-art theoretical simulations, even though they provide useful information about both the electronic structure and the excitonic pair excitations in these materials. With the present paper, we want to overcome this lack of knowledge.

In a recent article,[20] we discussed the one-particle excitation spectra of the TMOs MnO, FeO, CoO, and NiO extensively. Quasiparticle electronic structures were calculated within the G_0W_0 approximation on top of a generalized Kohn-Sham band structure that was obtained using the HSE03 hybrid functional.[25] Here, we go one step further and compute the macroscopic dielectric functions, which provide insight into both the optical absorption properties of the TMOs and the energy-loss spectra at vanishing momentum transfer. Apart from individual quasiparticle excitations, the optical absorption is governed by excitonic states. The screened electron-hole attraction, which is responsible for the formation of excitons, is fully taken into account in our calculations by

solving the Bethe-Salpeter equation[26,27] (BSE). This approach, which has been proven to be highly successful for simple sp semiconductors,[28–30] has recently been extended to magnetic systems.[31] The resulting optical spectra provide insight into the electronic structures of the TMOs in a large frequency range. Moreover, we are able to analyze the origin of the absorption peaks in the experimental data. We observe striking similarities in the response functions of all four oxides, which allows us to derive general trends for the dominating excitation and screening mechanisms in these materials.

The paper is organized as follows: In Sec. II, we introduce the theoretical methods and summarize the computational details. The electronic quasiparticle band structures of the TMOs are discussed briefly in Sec. III. In Sec. IV, the optical properties, i.e., dielectric functions, reflectivities, and absorption coefficients, are presented, and a detailed analysis of the spectra is given. Further, we compare our results to the available experimental data. In Sec. V, the loss functions of the TMOs are calculated and compared to electron-energy loss (EEL) and inelastic x-ray scattering (IXS) measurements. Finally, a short summary is given and conclusions are drawn in Sec. VI.

II. METHODS AND COMPUTATIONAL DETAILS

The macroscopic frequency-dependent dielectric function $\varepsilon(\omega)$ is the key quantity for various spectroscopies. Its real and imaginary parts describe the dispersion and absorption of light in matter and can be directly linked to the Fresnel reflectivity at normal incidence,

$$R(\omega) = \left| \frac{\sqrt{\varepsilon(\omega)} - 1}{\sqrt{\varepsilon(\omega)} + 1} \right|^2, \tag{1}$$

and the optical absorption coefficient which is given by the relation

$$\alpha(\omega) = \frac{2\omega}{c} \mathrm{Im} \sqrt{\varepsilon(\omega)}, \tag{2}$$

with c being the vacuum speed of light. EEL or IXS experiments, on the other hand, probe the imaginary part of the inverse frequency- and wave-vector-dependent microscopic dielectric function.[32] However, in the limit of vanishing momentum transfer, the loss function $-\mathrm{Im}\, \varepsilon^{-1}(\omega)$ can be derived from the macroscopic dielectric function according to the Adler-Wiser relation.[33,34]

The most essential prerequisite for the accurate calculation of the dielectric function is a reliable description of the electronic states, taking exchange and correlation effects into account. This holds, in particular, for materials that contain both itinerant s and p states and strongly localized d states, where the most simple (semi-)local exchange-correlation functionals fail and more advanced approaches have to be employed. To capture the one-particle excitation properties, e.g., the quasiparticle band gap, of the TMOs correctly, the GW method is applied. In a second step, we solve the BSE to take into account excitonic effects, i.e., the screened Coulomb interaction between the electrons and holes that are created in the optical excitation process. The Bethe-Salpeter ansatz permits us to include also the local-field effects to account for the inhomogeneity of the crystals.

A. Electronic structure

The electronic structures of the TMOs are computed using DFT and many-body calculations in the GW approximation as implemented in VASP.[35–37] The TM $3d$ and $4s$ orbitals as well as the oxygen $2s$ and $2p$ orbitals are considered as valence states. The electronic wave functions are expanded in plane waves up to cutoffs of 315 eV (MnO), 400 eV (FeO), 400 eV (CoO), and 325 eV (NiO), whereas the projector-augmented wave method is used to describe the electronic states in the vicinity of the ions.

In the calculations performed here, the small experimentally observed rhombohedral and tetragonal distortions[2,3,38] of the cubic rock-salt structure, which occur in the TMOs below the Néel temperature, are neglected. The resulting changes in the electronic structure, i.e., band splittings due to the lower symmetry of the distorted unit cells, are small and cannot be resolved in the optical absorption spectra. We assume lattice constants of 8.863 Å (MnO), 8.666 Å (FeO), 8.499 Å (CoO), and 8.341 Å (NiO), chosen such that the volume of the cubic cell coincides with the volume that is experimentally observed for the distorted structures.[2,3,39]

As demonstrated earlier,[20,31] the electronic structures of these materials can be well described by GW calculations in the perturbative G_0W_0 one-shot approach, starting from a generalized Kohn-Sham electronic structure that is computed self-consistently in DFT using the HSE03 (Ref. 25) hybrid density functional. For further details as well as for an elaborate discussion of the resulting band gaps, quasiparticle band structures, densities of states, and comparison to photoemission measurements, we refer to Ref. 20.

For the computation of the optical absorption and energy-loss spectra in a wide frequency range, the electronic states have to be calculated for a large number of bands and symmetry-inequivalent $\mathbf{k}$ points. However, the HSE03+G_0W_0 approach is too computer-time demanding to provide such a huge number of electronic states. To render this task computationally feasible, we mimic the sophisticated many-body calculation by the computationally less expensive GGA+U+Δ approach, where the band structure is calculated in the generalized-gradient approximation (GGA) with an additional on-site interaction U that acts only on d states.[14] The many-body effects which open the band gap are approximately taken into account by a scissors shift Δ. The two fitting parameters U and Δ are determined such that the best possible agreement (concerning the positions and intensities of the characteristic peaks in the density of states) with the HSE03+G_0W_0 electronic structure is obtained. Under these assumptions, we have derived values of $U = 2.0$ eV (MnO), 3.0 eV (FeO, CoO, NiO), and $\Delta = 3.0$ eV (MnO), 1.5 eV (FeO), 2.5 eV (CoO), and 2.0 eV (NiO). A detailed discussion of these values and the resulting electronic structures can be found in Ref. 20. It has already been proven that the GGA+U+Δ approach as described above provides reliable optical absorption spectra for a wide range of materials with d electrons, reaching from the open-shell system MnO[31] to ZnO[40], CdO[40], SnO_2[41], and InN[42] with fully occupied d states.

B. Dielectric function

For solving the BSE to obtain the dielectric function, we first set up the electron-hole pair Hamiltonian, which is determined by the quasiparticle states from the electronic band structure, the matrix elements of the screened electron-hole attraction, and the matrix elements of the bare Coulomb interaction to account for local-field effects.[28–30]

Since we are studying antiferromagnetic materials, the inclusion of the spin degree of freedom requires special care: (i) Singlet and triplet excitations are no longer well defined.[31] (ii) Optical excitations do not flip spins in the electric dipole approximation and the framework of collinear magnetism. Therefore, only vertical excitations from a valence band v to a conduction band c with the *same* spin quantum number m can take place, i.e., all independent electron-hole pair states can be labeled by $|cv\mathbf{k}m\rangle$.[31] This is crucial for the interpretation of absorption spectra of magnetic materials. (iii) The combination of both effects leads to an increase of the rank of the electron-hole pair Hamiltonian by a factor of 2, which renders computations even more expensive than for nonmagnetic materials.

Instead of diagonalizing the Hamiltonian, the eigenvalue problem is transformed into an initial-value problem which is solved my means of a time-evolution scheme.[43] This approach, which scales only quadratically with the rank of the Hamiltonian, yields the frequency-dependent dielectric function but does not provide access to individual excitonic eigenvalues or oscillator strengths.

The static dielectric screening that enters the matrix elements of the electron-hole attraction is calculated by means of an analytical expression that was suggested by Bechstedt *et al.*[44] It models the behavior of the dielectric screening in reciprocal space and depends on the electronic static dielectric constant ε_∞ and the average valence-electron density in the system. The values for $\varepsilon_\infty = 4.95$ (MnO),[45] 5.3 (CoO),[46,47] and 5.7 (NiO)[47] are taken from experiment. For FeO, a value of 5.0 is chosen following the chemical trend of the other materials, since the only available experimental result of 11.1 has been obtained for Fe_xO with a large iron deficit of several percent.[48] In order to consolidate the results, the optical absorption spectra have also been calculated using merely the dielectric constant, i.e., omitting the variation of the screening in reciprocal space completely, and no significant change in the spectra was observed. Further, the validity of the Tamm-Dancoff approximation, which is usually utilized for calculating optical spectra of bulk insulators, has been checked carefully and found to hold also for the TMOs.

In the two-particle Hamiltonian, transitions with independent-particle (GGA+U) energies up to 20 eV are included. The Brillouin zone is sampled with a regular $8 \times 8 \times 8$ **k**-point mesh that is shifted by $0.2 \times 0.3 \times 0.5$ times the distance between adjacent **k** points out of the symmetric positions. To ensure also the convergence of the real part of the dielectric function, which is linked to the imaginary part by a Kramers-Kronig transformation, the dielectric function above 20 eV is evaluated in the independent-quasiparticle approximation (IQPA) up to 80 eV and the contributions of the corresponding excitations to the real part below 20 eV are added to the BSE spectrum. A Lorentzian broadening of 0.15 eV is applied to the dielectric functions. The absorption coefficients of the TMOs are derived from the macroscopic dielectric functions according to Eq. (2).

Since the resolution of EEL spectra is generally lower and we are not interested in the fine structure of the edge, we can reduce the Brillouin-zone sampling to obtain the loss function $-\mathrm{Im}\ \varepsilon^{-1}(\omega)$ and take into account the electron-hole interaction up to higher transition energies instead. Hence, we use a mesh of $4 \times 4 \times 4$ shifted **k** points and solve the two-particle Hamiltonian up to transitions of 80 eV. For the loss spectra, a broadening of 0.5 eV is used. The reflectivity spectra are calculated according to Eq. (1) with the same set of convergence parameters as the loss spectra, since experimental data are available in a large spectral range, albeit with limited resolution.

III. QUASIPARTICLE BAND STRUCTURE

In order to demonstrate the reliability of the electronic structures which constitute the starting point of our response-function calculations, we compare the HSE03+G_0W_0 quasiparticle band structures from Ref. 20 with the quasiparticle band structures resulting from the GGA+U+Δ approach in Fig. 1. It is clearly visible that the GGA+U+Δ method reproduces all main features of the more sophisticated quasiparticle band structure with an accuracy that might be surprising for two methods that seem to be so different at first glance. However, the main driving force that opens the gap between the occupied and unoccupied d states is the screened exchange which is inherent in both approaches. The HSE03 energy functional contains a screened-exchange contribution, as does the GW self-energy operator. Even though inspired by the Hubbard model to treat the physics of correlated systems, the way in which on-site corrections to (semi-)local energy functionals are implemented in DFT functionals corresponds to a screened exchange interaction (see, e.g., the functional introduced by Dudarev *et al.*[14]). Furthermore, the scissors operator Δ is a first approximation to the gap opening caused by the self-energy in the GW approximation.

The general agreement between both approaches in the valence-band region is excellent. Only for FeO and CoO, the total width of the valence bands is slightly underestimated. The influence of this effect on the optical spectra is discussed in Sec. IV A3. For all four TMOs, the energetic positions of the O $2s$ states around -20 eV are slightly off compared to the HSE03+G_0W_0 approach. However, this is of minor importance for the optical spectra, since these states contribute only at energies above 20 eV to the absorption where the total oscillator strength is already very low. Also the conduction-band positions and dispersions obtained within the GGA+U+Δ approach match well those from the HSE03+G_0W_0 calculations, in particular with regard to the ordering of sp and d states. The scissors shifts are chosen to yield the best overall agreement with all conduction bands and not to reproduce the band gap as well as possible. This makes a slight overestimation of the band gaps in the GGA+U+Δ approach inevitable. As we are not interested in the fine details of the absorption edge, but in the spectra in a large frequency range, this is not a critical issue. Moreover, the absorption onsets, in contrast to other oxides (cf., e.g., Ref. 40 for MgO and ZnO), do not give

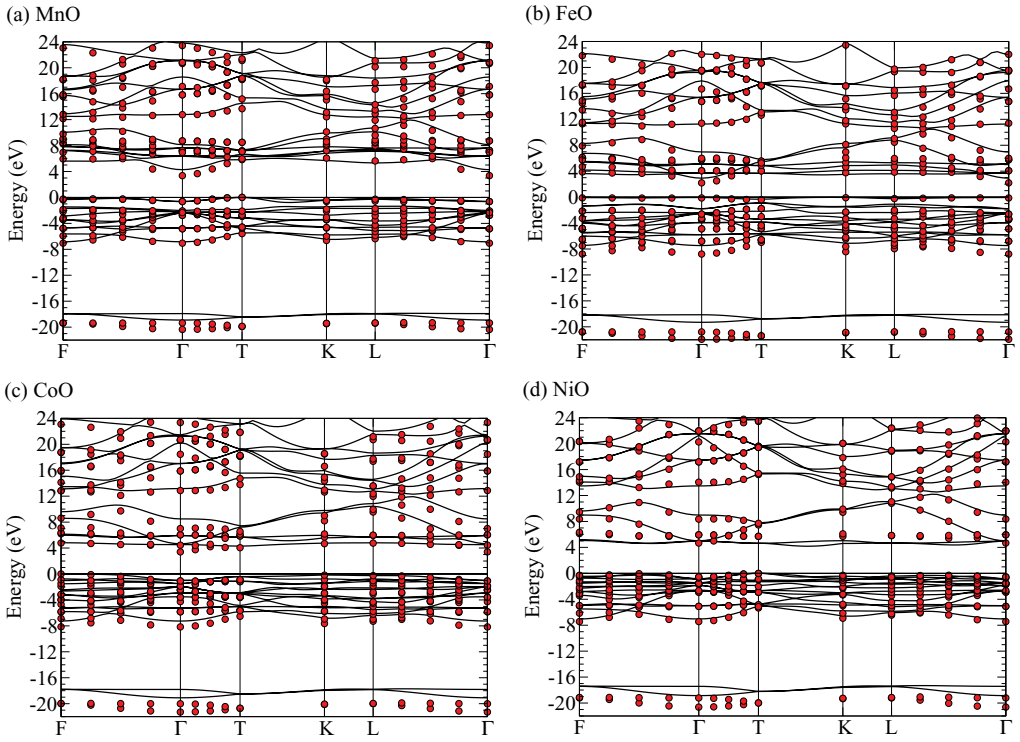

FIG. 1. (Color online) Quasiparticle band structures for MnO, FeO, CoO, and NiO. The solid lines represent the GGA+U+Δ bands, whereas the red dots denote the HSE03+G_0W_0 reference band structures from Ref. 20. The valence-band maximum is set to zero. The high-symmetry points of the Brillouin zone are labeled as in Ref. 49.

rise to prominent features such as strong exciton series in the absorption spectrum, since the densities of states in the vicinity of the conduction-band minima are comparably low[20] and the corresponding transitions are symmetry forbidden at the Γ point (see Sec. IV A2).

Eventually, it has to be stressed that the choice of the parameters U and Δ is not empirically motivated. They are derived by comparison to a parameter-free *ab initio* calculation and constitute a computationally cheap and accurate alternative to the full many-body calculation.

IV. OPTICAL PROPERTIES

A. Dielectric functions

1. General properties

In Fig. 2, the real and imaginary parts of the frequency-dependent dielectric function $\varepsilon(\omega)$ are shown for a wide frequency range up to 20 eV. They have been calculated in two approximations: (i) IQPA, where excitonic and local-field effects are neglected and the contributions to the optical absorption that arise from individual quasiparticle transitions in the GGA+U+Δ approach are merely summed up weighted by their respective oscillator strength, (ii) solving the BSE, taking additionally into account the influence of the local crystal fields and the static electron-hole attraction, i.e., the dominating many-body effect which is responsible for the occurrence of excitons.

The dielectric functions of the four TMOs in the IQPA have many features in common, which is due to their similar electronic structure. The low-energy part of Im $\varepsilon(\omega)$ is governed by a more or less structured absorption peak that dominates the whole spectrum. It mainly originates from transitions with d bands as initial and/or final states (see Sec. IV A2) and constitutes basically the only characteristic absorption feature. Above ∼8 eV, the spectra are continued by a rather structureless plateau that declines slowly at higher energies.

The inclusion of excitonic effects by solving the BSE leads to a strong overall redshift of the absorption spectra by about 1 eV and an enhancement of the peaks at low energies, whereas the general line shape of Im $\varepsilon(\omega)$ is retained. The redshift is an effect that is well known from simple nonmagnetic semiconductors, even though its magnitude is often smaller in these materials.[28,53] In contrast to other monoxides, such as MgO and ZnO,[40] we do not observe line-shape modifications that are due to the formation of Wannier-Mott-like excitons within the quasiparticle band gap or at other critical points within the interband continuum. In the TMOs, the bands are rather flat and we do not find pronounced parabolic band edges that are indispensable prerequisites for the occurrence of Wannier-Mott excitons.

However, there is experimental evidence for Frenkel-like excitonic bound states within the fundamental band gap. Even though optical spectroscopy is not able to probe those excitons directly, they are visible in EEL spectroscopy (EELS) and nonresonant IXS experiments[54] for large transferred momenta $\mathbf{q}$ or in resonant IXS,[55] where other selection rules hold. These excitons, which are mainly due to intra-atomic d-d excitations, cannot be observed in optical absorption spectra, since they are forbidden by the dipole selection rule for the orbital quantum

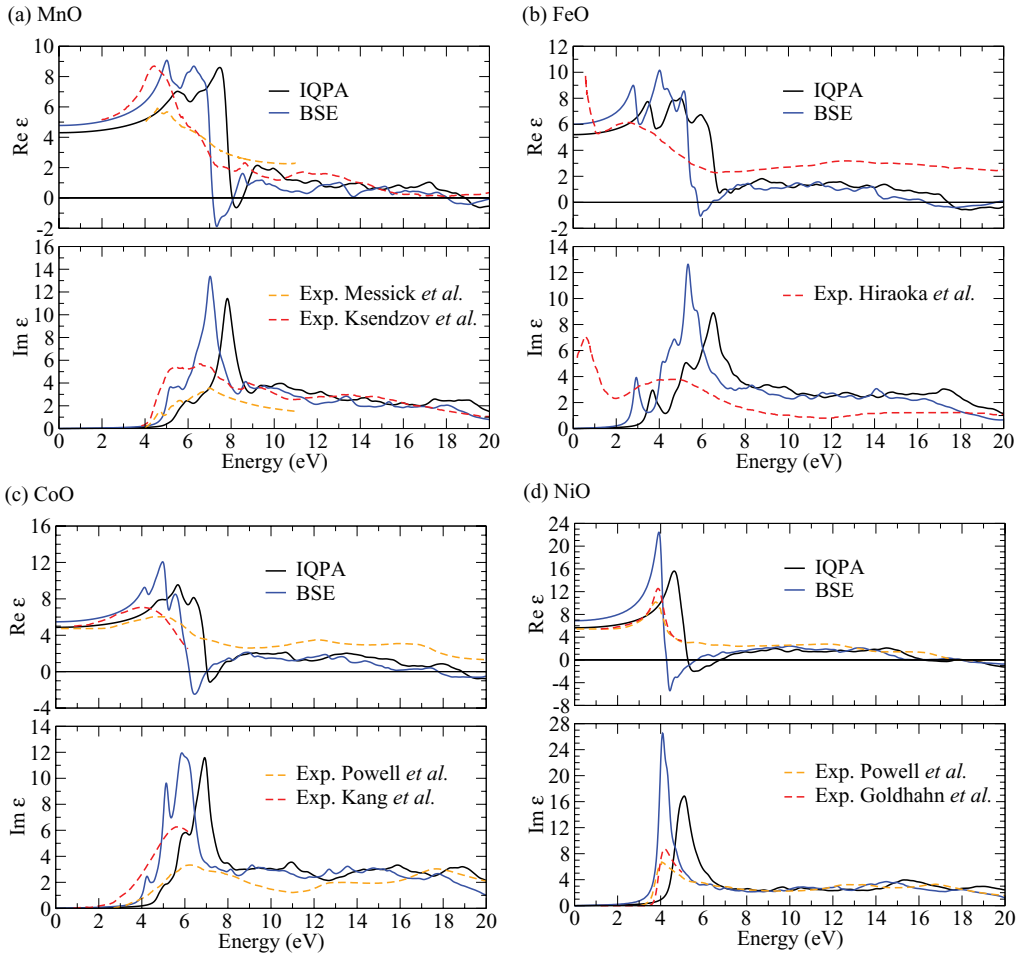

FIG. 2. (Color online) Real and imaginary parts of the frequency-dependent macroscopic dielectric function $\varepsilon(\omega)$ for MnO, FeO, CoO, and NiO calculated in the independent-quasiparticle approximation (IQPA) and solving the Bethe-Salpeter equation (BSE). Experimental spectra that are derived from reflectivity (Messick *et al.*,[22] Ksendzov *et al.*,[23] Hiraoka *et al.*,[50] and Powell and Spicer[24]) or ellipsometry (Kang *et al.*[51] and Goldhahn and Schley[52]) measurements are shown for comparison. The spectrum of FeO from Hiraoka *et al.* is biased by strong defect absorption at low frequencies due to the nonstoichiometry of the sample.[50]

number $\Delta l = \pm 1$. Some of these excitations additionally require spin flips which are also dipole forbidden within the framework of collinear spins. Only by inclusion of spin-orbit coupling, they might become weakly allowed. Indeed, they are found in low-energy absorption experiments[56–58] but cannot be distinguished unambiguously from possible defect absorption.

The influence of local-field effects on the optical absorption, which usually leads to a blueshift of the spectra, is negligible for the TMOs, as has already been shown for MnO in Ref. 31. Even though these materials are locally very inhomogeneous because of the ionic nature of the crystals, these localized charges are not easily polarizable. The electrons are not able to screen external fields efficiently, since they are bound tightly to the ions. This argument is confirmed by the small differences between the electronic static microscopic and macroscopic dielectric constants of the TMOs (see Table III of Ref. 20).

2. *Allowed and forbidden transitions*

Traditionally, the low-energy parts of the TMO absorption spectra have been interpreted in an atomic picture in terms of transitions between multiplets of the TM 3*d* states along with the corresponding selection rules.[22,24,59] We would like to point out the pitfalls of such an approach and show to what extent it can be misleading.

A detailed analysis of the absorption peaks is always hampered by the overlap and hybridization of *s*, *p*, and *d* states in both the valence and conduction bands. Here, we concentrate on the lowest-energy transitions of MnO and NiO as generic examples, because in these materials the *d* and *s* bands at the band edges can be rather easily disentangled from bands with other symmetries. In the left panels of Fig. 3, the imaginary parts of the dielectric functions for MnO and NiO in the IQPA are shown and the contributions of selected interband transitions are highlighted. The optical transition matrix elements $|\mathbf{p}|^2$ for each of these interband transitions have been calculated in the longitudinal approach following Gajdoš *et al.*[60] They are plotted along high-symmetry lines of the Brillouin zone together with the corresponding band structures in the right panels of Fig. 3.

For MnO, the contributions to the optical absorption that arise from transitions between the occupied e_g and the empty *s* states, as well as between the occupied e_g and the empty t_{2g} states, are depicted. It is obvious that the low-energy part

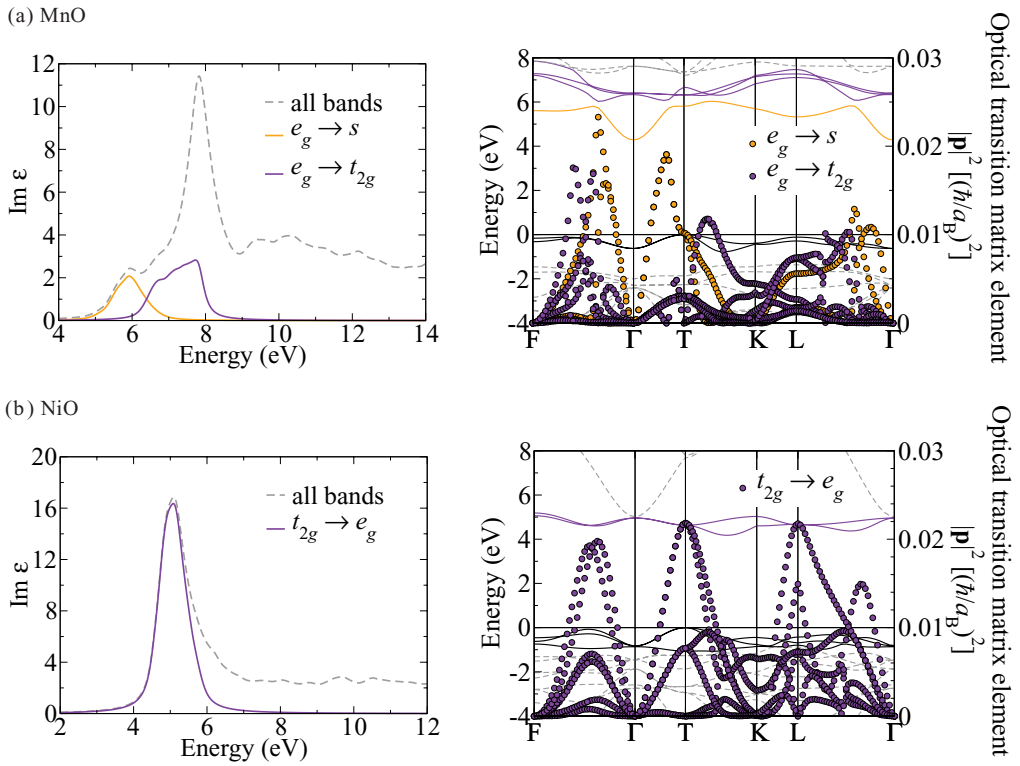

FIG. 3. (Color online) Analysis of the transitions that contribute to the main absorption peaks of MnO (a) and NiO (b). In the left panels, the imaginary parts of the dielectric functions in IQPA (all bands) are shown together with the contributions of the $e_g \rightarrow s$ and $e_g \rightarrow t_{2g}$ (MnO) or $t_{2g} \rightarrow e_g$ transitions (NiO). In the right panels, the corresponding states in the band structures are highlighted. The black solid lines indicate the valence-band e_g (MnO) or t_{2g} states (NiO). The final states of the respective optical transitions are shown in the same colors as the partial optical spectra in the left panels. Furthermore, the right panels depict the optical transition matrix elements $|\mathbf{p}|^2$ for the interband transitions (dotted curves) along the Brillouin-zone path. It is clearly visible that interband transitions which are forbidden at the Γ point for symmetry reasons can contribute strongly to the optical absorption in other parts of the Brillouin zone.

of the absorption spectrum is entirely due to these transitions which are *forbidden* in atoms because they violate the selection rule $\Delta l = \pm 1$. Indeed, the corresponding transition matrix elements are zero at the Γ point [see right panel of Fig. 3(a)]. However, these interband transitions are dipole *allowed* in the rest of the Brillouin zone. Even though the transition matrix elements are one order of magnitude smaller than for sp-bonded semiconductors[61] or other oxide insulators,[62] they are nevertheless responsible for the whole optical spectral strength at low energies. It has to be stressed that the $e_g \rightarrow t_{2g}$ transitions are interatomic transitions between Mn atoms of opposite spin polarization, since intra-atomic excitations would require spin flips and thus violate the spin selection rule. This may be the reason for their comparably low oscillator strength. Due to the high joint density of states of these flat bands, we yet find significant peaks in the absorption spectrum.

The case of NiO is even more striking. The only feature of the absorption spectrum, the peak at 5 eV in the IQPA spectrum, stems entirely from transitions between the occupied t_{2g} and the unoccupied e_g minority-spin d states. Also, these transitions are symmetry forbidden at the Γ point but contribute to the absorption in large parts of the Brillouin zone. In contrast to MnO, these excitations are mainly intra-atomic which may explain, together with a high joint density of states, their bigger oscillator strength.

Hence, we conclude that an interpretation of the optical spectra of the TMOs in terms of purely atomic models can be highly deceptive and has to be handled with extreme care. It might be suitable for the Frenkel-like excitons within the band gap, but not for the analysis of the interband continuum.

3. *Comparison to experiments*

The optical absorption of MnO is governed by a two-peak structure [see Fig. 2(a)]. The first peak, that is found at 5.3 eV when excitonic and local-field effects are included in the calculation, is due to $e_g \rightarrow s$ transitions, while the second and largest peak of the whole spectrum at 7.0 eV stems from $e_g \rightarrow t_{2g}$, $e_g \rightarrow e_g$, and $t_{2g} \rightarrow s$ transitions, which are all symmetry forbidden in an atomic picture. The plateau at higher energies originates from various interband transitions that involve also the O $2p$ states. The experimental spectra for Im $\varepsilon(\omega)$ are derived from near-normal-incidence reflectivity measurements by Kramers-Kronig transformation.[22,23] Both measured curves exhibit the characteristic two-peak structure that has also been found in our calculations and the peak positions agree well with our results. However, we observe significant differences in the peak intensities both between the two experimental curves and between the experimental curves and our calculations. Possible reasons might be sample-quality problems of these rather old

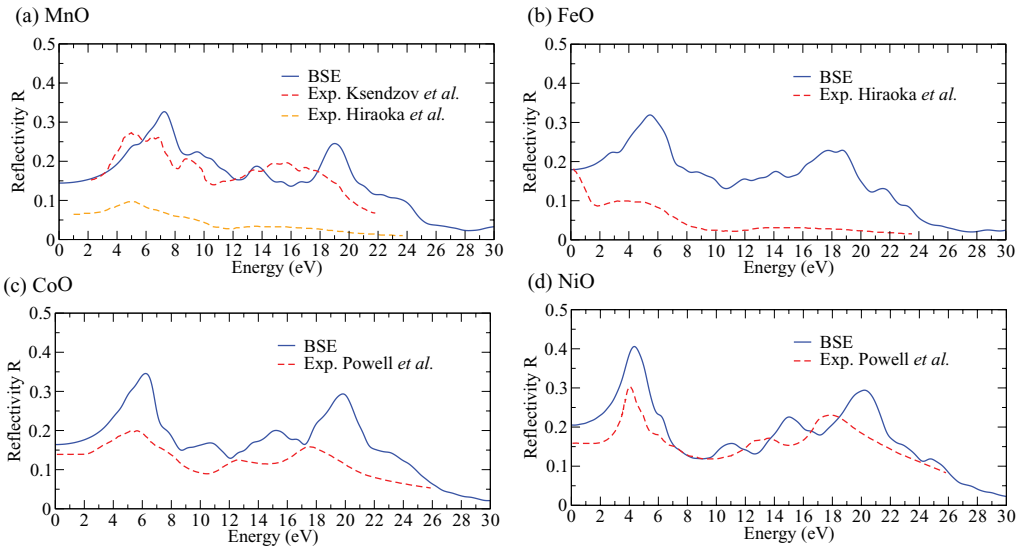

FIG. 4. (Color online) Reflectivities for MnO, FeO, CoO, and NiO at normal incidence. The spectra have been calculated by solving the Bethe-Salpeter equation (BSE) including excitonic and local-field effects. The experimental data are taken from Ksendzov *et al.*,[23] Hiraoka *et al.*,[50] and Powell and Spicer.[24] The reflectivity spectrum of FeO from Hiraoka *et al.* is biased by strong defect absorption at low frequencies due to the nonstoichiometry of the sample.[50]

data (defect states, surface roughness) or assumptions about the high-energy behavior of the dielectric function that enter the Kramers-Kronig transformation. However, the high-energy part of the calculated spectrum and the data of Ksendzov *et al.*[23] match almost perfectly. Also, the real part of $\varepsilon(\omega)$ agrees well with the measurements of Ksendzov *et al.*, except for the intensity of the second peak.

The imaginary part of the dielectric function of FeO solving the BSE [Fig. 2(b)] exhibits a small peak at 2.9 eV which arises from transitions with initial states in the single filled minority-spin t_{2g} band. It is followed by the main structure of the absorption spectrum. It is not possible to disentangle individual contributions to this prominent feature, because the involved valence p and d as well as conduction s and d states strongly overlap. Experimental data for the stoichiometric monoxide FeO are not available, since it is not stable in nature. Hiraoka *et al.*[50] recently reported on an optical absorption spectrum derived from reflectivity data for Fe_xO with an iron deficiency of several percent. It exhibits a strong absorption peak within the fundamental gap of FeO which the authors assign to defect absorption at Fe vacancies in their samples. Even though the experimental resolution is not very high, the measured data possess a broad peak in the vicinity of 4.5 eV and a plateau at higher energies that match our calculated spectra. The overestimation of the total peak height might be partially due to the mentioned underestimation of the valence-band width (cf. Sec. III). Other issues are, of course, the nonstoichiometry of the sample and the experimental resolution. Within the limitations discussed above, the real part of $\varepsilon(\omega)$ agrees well with the data of Hiraoka *et al.*, except for the strong rise at low energies in the experimental curve that is due to defect absorption.

Also in the case of CoO, the imaginary part of $\varepsilon(\omega)$ features a broad and intense peak at low energies that cannot be analyzed straightforwardly in terms of individual transitions [see Fig. 2(c)]. The experimental data of Powell and Spicer[24] from reflectivity measurements and Kang *et al.*[51] from spectroscopic ellipsometry both exhibit this absorption peak, albeit with strongly deviating intensity. We find better agreement with the more recent data concerning peak intensity, even though it still seems to be overestimated by our calculations, which might again be in part due to the underestimation of the valence-band width in the band-structure calculations (cf. Sec. III). However, the positions of the absorption peaks match those found by Powell and Spicer, whereas the curve of Kang *et al.* seems to be redshifted. The real parts of $\varepsilon(\omega)$ agree well with the experimental data, taking into account instrumental, temperature, and lifetime broadening effects.

As already discussed above, the optical absorption of NiO [Figs. 2(d) and 3(b)] is dominated by intra-atomic $t_{2g} \rightarrow e_g$ transitions. The experimental data which are derived from reflectivity[24] and ellipsometry measurements[52] agree very well with the calculated curves solving the BSE in the whole studied spectral range. Only concerning the intensity of the main absorption peak, we observe significant deviations. For NiO with its particularly simply shaped absorption spectrum, the necessity to include excitonic effects in the calculation of the optical absorption is most obvious, since the main absorption peak in the IQPA deviates significantly from the measured position.

Besides the experimental issues already discussed, we would like to point out other possible reasons for the overestimation of the peak intensities in all TMOs. The neglect of local-field contributions to the dielectric function that enters the screened electron-hole interaction may lead to an underestimation of the screening and, therefore, to an artificially increased peak enhancement when going from the IQPA to the full solution of the BSE. Further, the presence of free carriers in the samples due to defects or natural doping (for instance, Kang *et al.*[51] report on excess oxygen and Hiraoka

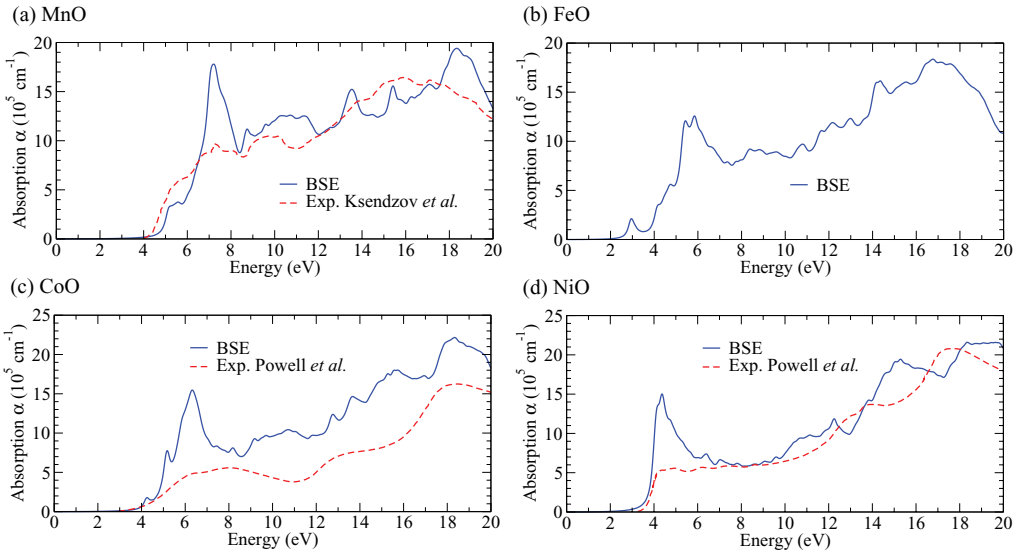

FIG. 5. (Color online) Absorption coefficients for MnO, FeO, CoO, and NiO. The spectra have been calculated by solving the Bethe-Salpeter equation (BSE) including excitonic and local-field effects. The experimental curves from Ksendzov *et al.*[23] and Powell and Spicer[24] have been derived from reflectivity data.

et al.[50] on iron deficiencies) may cause a screening of the excitonic effects in experiment.[63]

B. Reflectivities and absorption coefficients

Most optical experiments actually probe reflectivities R or absorption coefficients α. The real and imaginary parts of the dielectric function are only deduced therefrom by Kramers-Kronig transformation or similar methods with additional assumptions on the analytical behavior of the dielectric function for very small and large frequencies. Therefore, we have also calculated the normal-incidence reflectivities and absorption coefficients including excitonic and local-field effects in a large spectral range and compared the results to available experimental data in Figs. 4 and 5.

The reflectivity spectra of all four oxides basically exhibit a two-peak structure with a first peak that corresponds to the dominant peaks in Im $\varepsilon(\omega)$ and a second one in the vicinity of 20 eV right before the onset of the plasmon excitations (see Sec. V). The agreement between the computed spectra and the experimental data from Ksendzov *et al.*[23] and Powell and Spicer[24] is reasonable, taking into account the sensitivity of reflectivity measurements to surface roughness and oxidation. Only the intensity of the spectra from Hiraoka *et al.*[50] deviates significantly. The considerably lower reflectivity both compared to our calculations and other experiments may possibly be traced back to measuring the polar (111) surface which is subject to surface passivation, e.g., by oxidation. In the case of FeO, the nonstoichiometry of the sample also has to be kept in mind.

The calculated absorption onsets as well as the general line shape of the frequency-dependent absorption coefficients (see Fig. 5) agree well with the experimental spectra for MnO and NiO. Only the intensities of the pronounced peaks in Im $\varepsilon(\omega)$ are overestimated for all TMOs, as has already been discussed above. For CoO, the computed optical absorption coefficient is higher than the measured spectrum throughout the whole frequency range. However, the qualitative behavior of the absorption is well reproduced.

V. ENERGY-LOSS SPECTRA

In Fig. 6, we present the energy-loss functions $-\mathrm{Im}\ \varepsilon^{-1}(\omega)$ of the TMOs. The loss spectra including excitonic and local-field effects at vanishing momentum transfer can be obtained directly by inversion of the macroscopic dielectric function. The loss function is related to the dynamical structure factor $S(\mathbf{q},\omega)$, which can be probed in EEL and IXS experiments, by means of

$$-\mathrm{Im}\ \varepsilon^{-1}(\mathbf{q},\omega) = \pi v(\mathbf{q}) S(\mathbf{q},\omega), \tag{3}$$

with the Coulomb potential in reciprocal space $v(\mathbf{q})$ and the momentum transfer $\mathbf{q}$. Here, we concentrate on the loss in the limit of vanishing momentum $\mathbf{q} = 0$.

The loss spectra of the TMOs in Fig. 6 resemble each other strongly, which is due to the similar electronic structures of these four materials. Especially the dominant loss peaks in the energy range between 20 and 25 eV exhibit similar line shapes, intensities, and peak positions. The steep rise of the loss function at the low-energy edge of this broad feature coincides with a zero in Re $\varepsilon(\omega)$ at 20.2 (MnO), 19.6 (FeO), 21.5 (CoO), and 22.0 eV (NiO), which corresponds to the longitudinal plasma frequency. Consequently, these peaks represent collective charge oscillations of the valence-electron gas. As the slopes of the real parts of the dielectric functions in the vicinity of the zeros are extremely small, we find in each of the TMOs a very broad feature that is extended over several electronvolts and possesses a fine structure. For the same reason, the exact values of the zeros depend sensitively on the convergence parameters.

The classical plasma frequency $\omega_\mathrm{p} = \sqrt{e^2 n/(\varepsilon_0 m)}$ (with n the average valence-electron density, e the elementary charge, m the electron mass, and ε_0 the vacuum dielectric constant) of

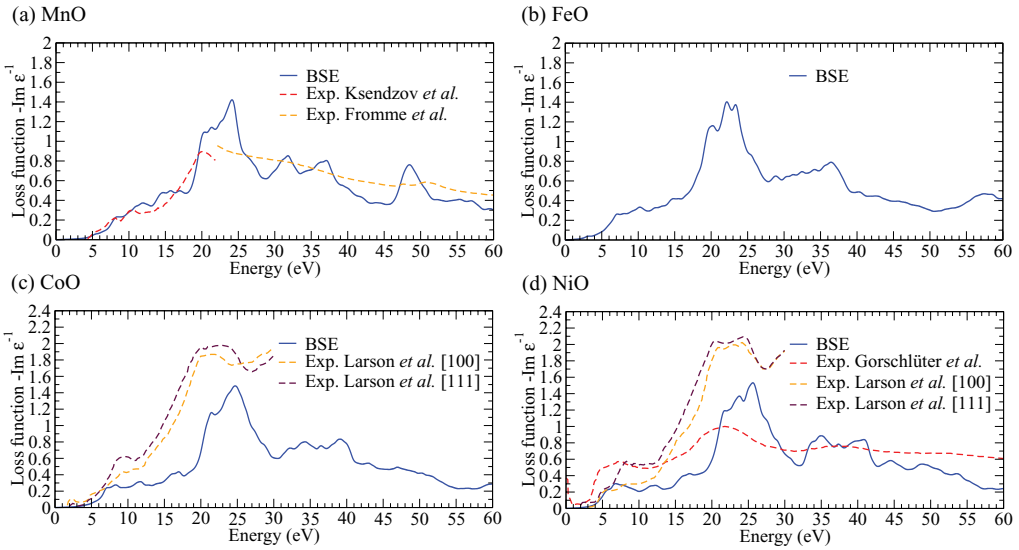

FIG. 6. (Color online) Energy-loss spectra for MnO, FeO, CoO, and NiO at vanishing momentum transfer, including excitonic and local-field effects (BSE). The experimental reference data have been derived from reflectivity measurements (Ksendzov *et al.*[23]), EELS (Fromme *et al.*,[64] Gorschlüter and Merz[65]) of the MnO and NiO (100) surfaces, and IXS of CoO and NiO along the [100] and [111] directions (Larson *et al.*[54]). The curves from Fromme *et al.* and Gorschlüter and Merz are plotted in arbitrary units.

the O $2p$ and TM $4s$ valence electrons amounts to $\hbar\omega_p = 19.5$ (MnO), 20.2 (FeO), 20.8 (CoO), and 21.4 eV (NiO). If also the TM $3d$ electrons are assumed to contribute fully to the dielectric screening, we obtain 26.4 (MnO), 28.5 (FeO), 30.6 (CoO), and 32.6 eV (NiO) instead. Finally, including also the O $2s$ electrons in the valence-electron density yields $\hbar\omega_p =$ 28.7 (MnO), 30.8 (FeO), 32.8 (CoO), and 34.9 eV (NiO). The actual plasma frequencies derived from the zeros in $\mathrm{Re}\,\varepsilon(\omega)$ agree surprisingly well with the classical plasma frequencies which take only the O $2p$ and TM $4s$ electrons into account. This leads us to the conclusion that the TM $3d$ electrons and even more so the O $2s$ electrons contribute to the lowest-energy collective charge excitations in the TMOs at most partially, since they are bound tightly to the atoms. However, the broad peaks in the loss functions continue above the longitudinal plasma frequencies and possess a considerable fine structure. This may be due to successive contributions of the TM $3d$ electrons (above ∼25 eV) and O $2s$ electrons (above ∼30 eV) to the plasma oscillations.

In Fig. 6(a), the loss spectrum of MnO is compared to experimental results that were obtained from reflectivity data[23] at low energies and direct EEL measurements for finite momentum transfer[64] at much higher energies. The high-energy part of the experimental loss spectrum can be assumed not to depend strongly on the wave vector and can thus be compared to the calculated curve at $\mathbf{q} = 0$ in a very rough first approximation. Unfortunately, the available experimental data do not cover the most interesting spectral range that contains the broad plasmon peak. The calculated spectrum including excitonic and local-field effects matches excellently the experimental curve in the range of the interband transitions below the longitudinal plasma frequency. The measured loss spectrum in the high-energy range is in arbitrary units and is almost featureless due to strong broadening effects, yet the general line shape and the positions of the very faint peaks agree well with the calculated spectrum.

Recently, nonresonant IXS measurements for CoO and NiO have been performed by Larson *et al.*[54] The resulting frequency-dependent structure factors $S(\mathbf{q},\omega)$ have been converted to loss functions according to Eq. (3). They are plotted for low momentum transfers $\mathbf{q} = 2\ \text{Å}^{-1}$ along two reciprocal directions in Figs. 6(c) and 6(d) together with the calculated loss spectra for $\mathbf{q} = 0$. The direction dependence of the measured curves is rather low for such small $\mathbf{q}$. The IXS data feature a pronounced loss peak whose position and line shape agree very well with the calculated loss spectra including excitonic and local-field effects for both CoO and NiO. Larger discrepancies are observed for the interband-transition region, which is most likely due to the stronger $\mathbf{q}$ dependence of the loss at lower energies and the fact that the measured data were obtained for small but nonvanishing momentum. For NiO, single-crystal EEL spectra have been reported by Gorschlüter and Merz.[65] The EELS data are in arbitrary units and have a significantly lower resolution than the IXS measurements. However, the main features of the loss function can also be identified and their positions agree fairly with the computed spectra. The overestimation of the spectral strength in the interband region is most likely again due to the nonvanishing transferred momentum in the experiments.

VI. SUMMARY AND CONCLUSIONS

In this paper, we have studied the optical and energy-loss properties of the antiferromagnetic TMOs MnO, FeO, CoO, and NiO using many-body perturbation theory. The *ab initio* calculations are based on reliable quasiparticle band structures that have been obtained previously in the HSE03+G_0W_0 approach. To reduce the computational effort and render the many-body calculations of the optical absorption spectra feasible, these sophisticated band structures were mimicked by means of the computationally less demanding GGA+U+Δ method. Subsequently, the BSE was solved to

obtain the frequency-dependent dielectric functions including excitonic and local-field effects in a wide spectral range. These dielectric functions were converted to reflectivities and optical absorption coefficients and compared to experimental data. Furthermore, the loss spectra at vanishing momentum transfer were also discussed.

In the TMOs, the screened electron-hole attraction leads to a strong redshift of the optical absorption peaks compared to the independent-quasiparticle approach. It has been shown that the inclusion of excitonic effects is indispensable to obtain agreement with the experimentally observed absorption-peak positions. The analysis of the absorption spectra in terms of contributing single-particle excitations reveals that the optical properties of the TMOs cannot be explained in a purely atomic picture. In reality, itinerant *s* and *p* states and localized *d* orbitals strongly overlap energetically and have to be treated on a common footing. We have shown that first-principles calculations that capture the full quasiparticle band structure as well as the electron-hole interaction are necessary. Open questions concerning the systematic overestimation of the absorption-peak intensities in our calculations remain. It cannot be excluded that improved theoretical methods have to be employed that take into account the many-body interactions on a more advanced level. On the other hand, also the discrepancies between different experimental data for one and the same material are surprisingly high, which is most likely due to sample-preparation problems.

ACKNOWLEDGMENTS

Helpful discussions with F. Fuchs, A. Schleife, R. Goldhahn, and P. Schley are gratefully acknowledged. This work was financially supported by the Deutsche Forschungsgemeinschaft (Project No. Be1346/20-1) and the European Community within the framework of the ETSF (Grant No. 211956).

[1] P. A. Cox, *Transition Metal Oxides. An Introduction to their Electronic Structure and Properties*, The International Series of Monographs on Chemistry (Clarendon Press, Oxford, 1995).
[2] A. K. Cheetham and D. A. O. Hope, Phys. Rev. B **27**, 6964 (1983).
[3] W. Jauch, M. Reehuis, H. J. Bleif, F. Kubanek, and P. Pattison, Phys. Rev. B **64**, 052102 (2001).
[4] A. Schrön, C. Rödl, and F. Bechstedt, Phys. Rev. B **86**, 115134 (2012).
[5] J. H. de Boer and E. J. W. Verwey, Proc. Phys. Soc. **49**, 59 (1937).
[6] N. F. Mott and R. Peierls, Proc. Phys. Soc. **49**, 72 (1937).
[7] A. Fujimori and F. Minami, Phys. Rev. B **30**, 957 (1984).
[8] X. Ren, I. Leonov, G. Keller, M. Kollar, I. Nekrasov, and D. Vollhardt, Phys. Rev. B **74**, 195114 (2006).
[9] J. Kuneš, V. I. Anisimov, S. L. Skornyakov, A. V. Lukoyanov, and D. Vollhardt, Phys. Rev. Lett. **99**, 156404 (2007).
[10] P. Hohenberg and W. Kohn, Phys. Rev. B **136**, 864 (1964).
[11] W. Kohn and L. J. Sham, Phys. Rev. A **140**, 1133 (1965).
[12] K. Terakura, T. Oguchi, A. R. Williams, and J. Kübler, Phys. Rev. B **30**, 4734 (1984).
[13] V. I. Anisimov, J. Zaanen, and O. K. Andersen, Phys. Rev. B **44**, 943 (1991).
[14] S. L. Dudarev, G. A. Botton, S. Y. Savrasov, C. J. Humphreys, and A. P. Sutton, Phys. Rev. B **57**, 1505 (1998).
[15] C. Franchini, V. Bayer, R. Podloucky, J. Paier, and G. Kresse, Phys. Rev. B **72**, 045132 (2005).
[16] M. Marsman, J. Paier, A. Stroppa, and G. Kresse, J. Phys.: Condens. Matter **20**, 064201 (2008).
[17] L. Hedin, Phys. Rev. A **139**, 796 (1965).
[18] S. V. Faleev, M. van Schilfgaarde, and T. Kotani, Phys. Rev. Lett. **93**, 126406 (2004).
[19] F. Fuchs, J. Furthmüller, F. Bechstedt, M. Shishkin, and G. Kresse, Phys. Rev. B **76**, 115109 (2007).
[20] C. Rödl, F. Fuchs, J. Furthmüller, and F. Bechstedt, Phys. Rev. B **79**, 235114 (2009).
[21] H. Jiang, R. I. Gomez-Abal, P. Rinke, and M. Scheffler, Phys. Rev. B **82**, 045108 (2010).
[22] L. Messick, W. C. Walker, and R. Glosser, Phys. Rev. B **6**, 3941 (1972).
[23] Y. M. Ksendzov, I. L. Korobova, K. K. Sidorin, and G. P. Startsev, Fiz. Tverd. Tela (Leningrad) **18**, 173 (1976).
[24] R. J. Powell and W. E. Spicer, Phys. Rev. B **2**, 2182 (1970).
[25] J. Heyd, G. E. Scuseria, and M. Ernzerhof, J. Chem. Phys. **118**, 8207 (2003).
[26] E. E. Salpeter and H. A. Bethe, Phys. Rev. **84**, 1232 (1951).
[27] G. Onida, L. Reining, and A. Rubio, Rev. Mod. Phys. **74**, 601 (2002).
[28] S. Albrecht, L. Reining, R. Del Sole, and G. Onida, Phys. Rev. Lett. **80**, 4510 (1998).
[29] L. X. Benedict, E. L. Shirley, and R. B. Bohn, Phys. Rev. Lett. **80**, 4514 (1998).
[30] M. Rohlfing and S. G. Louie, Phys. Rev. Lett. **81**, 2312 (1998).
[31] C. Rödl, F. Fuchs, J. Furthmüller, and F. Bechstedt, Phys. Rev. B **77**, 184408 (2008).
[32] P. Nozières and D. Pines, Phys. Rev. **113**, 1254 (1959).
[33] S. L. Adler, Phys. Rev. **126**, 413 (1962).
[34] N. Wiser, Phys. Rev. **129**, 62 (1963).
[35] G. Kresse and J. Furthmüller, Comput. Mater. Sci. **6**, 15 (1996), http://www.sciencedirect.com/science/article/B6TWM-3VRVTBF-3/2/88689b1e acfe2b5fe57f09d37eff3b74.
[36] G. Kresse and D. Joubert, Phys. Rev. B **59**, 1758 (1999).
[37] M. Shishkin and G. Kresse, Phys. Rev. B **74**, 035101 (2006).
[38] W. L. Roth, Phys. Rev. **110**, 1333 (1958).
[39] B. Hentschel, Z. Naturforsch. A **25**, 1996 (1970).
[40] A. Schleife, C. Rödl, F. Fuchs, J. Furthmüller, and F. Bechstedt, Phys. Rev. B **80**, 035112 (2009).
[41] A. Schleife, J. B. Varley, F. Fuchs, C. Rödl, F. Bechstedt, P. Rinke, A. Janotti, and C. G. Van de Walle, Phys. Rev. B **83**, 035116 (2011).
[42] F. Fuchs, C. Rödl, A. Schleife, and F. Bechstedt, Phys. Rev. B **78**, 085103 (2008).
[43] W. G. Schmidt, S. Glutsch, P. H. Hahn, and F. Bechstedt, Phys. Rev. B **67**, 085307 (2003).
[44] F. Bechstedt, R. Del Sole, G. Cappellini, and L. Reining, Solid State Commun. **84**, 765 (1992).
[45] J. N. Plendl, L. C. Mansur, S. S. Mitra, and I. F. Chang, Solid State Commun. **7**, 109 (1969).

[46]P. J. Gielisse, J. N. Plendl, L. C. Mansur, R. Marshall, S. S. Mitra, R. Mykolajewycz, and A. Smakula, J. Appl. Phys. **36**, 2446 (1965).
[47]S. Mochizuki and M. Satoh, Phys. Status Solidi B **106**, 667 (1981).
[48]B. Prévot, J. Biellmann, M. F. Meftah, and M. Sieskind, Phys. Status Solidi A **40**, 503 (1977).
[49]J. E. Pask, D. J. Singh, I. I. Mazin, C. S. Hellberg, and J. Kortus, Phys. Rev. B **64**, 024403 (2001).
[50]N. Hiraoka, H. Okamura, H. Ishii, I. Jarrige, K. D. Tsuei, and Y. Q. Cai, Eur. Phys. J. B **70**, 157 (2009).
[51]T. D. Kang, H. S. Lee, and H. Lee, J. Korean Phys. Soc. **50**, 632 (2007).
[52]R. Goldhahn and P. Schley (unpublished).
[53]L. X. Benedict, E. L. Shirley, and R. B. Bohn, Phys. Rev. B **57**, R9385 (1998).
[54]B. C. Larson, W. Ku, J. Z. Tischler, C.-C. Lee, O. D. Restrepo, A. G. Eguiluz, P. Zschack, and K. D. Finkelstein, Phys. Rev. Lett. **99**, 026401 (2007).
[55]L.-C. Duda, T. Schmitt, M. Magnuson, J. Forsberg, A. Olsson, J. Nordgren, K. Okada, and A. Kotani, Phys. Rev. Lett. **96**, 067402 (2006).
[56]R. N. Iskenderov, I. A. Drabkin, L. T. Emel'yanova, and Y. M. Ksendzov, Fiz. Tverd. Tela (Leningrad) **10**, 2573 (1968).
[57]G. W. Pratt, Jr. and R. Coelho, Phys. Rev. **116**, 281 (1959).
[58]R. Newman and R. M. Chrenko, Phys. Rev. **114**, 1507 (1959).
[59]W. A. Harrison, *Electronic Structure and the Properties of Solids* (Dover, New York, 1989).
[60]M. Gajdoš, K. Hummer, G. Kresse, J. Furthmüller, and F. Bechstedt, Phys. Rev. B **73**, 045112 (2006).
[61]P. Y. Yu and M. Cardona, *Fundamentals of Semiconductors*, 3rd ed. (Springer, Berlin, 2005).
[62]A. Schleife, F. Fuchs, C. Rödl, J. Furthmüller, and F. Bechstedt, Phys. Status Solidi B **246**, 2150 (2009).
[63]A. Schleife, C. Rödl, F. Fuchs, K. Hannewald, and F. Bechstedt, Phys. Rev. Lett. **107**, 236405 (2011).
[64]B. Fromme, U. Brunokowski, and E. Kisker, Phys. Rev. B **58**, 9783 (1998).
[65]A. Gorschlüter and H. Merz, Int. J. Mod. Phys. B **7**, 341 (1993).